Supplementary Information for

Rotary catalysis of bovine mitochondrial F$_1$-ATPase studied by single-molecule experiments

Ryohei Kobayashi, Hiroshi Ueno, Chun-Biu Li, Hiroyuki Noji

Corresponding author: Hiroyuki Noji
Email: hnoji@appchem.t.u-tokyo.ac.jp

This PDF file includes:

Supplementary text
Figs. S1 to S10
Table S1
References for SI reference citations

Supplementary Information Text

Change-Point (CP) analysis

Detection of Change point (CP) from rotary traces. We employed a nonparametric CP analysis based on permutation test (1) to identify angular changes in the single F_1 rotary traces. A CP is defined as the time point where an abrupt change occurs in the rotary angle. The main procedures in CP detection are as follows. Starting from a segment of rotary trace $(\theta_1, \theta_2, \cdots, \theta_n)$ with n time points and mean $\bar{\theta}$, the existence of a CP was examined using permutation test with two hypotheses: no CP exists (null hypothesis) versus at least one CP exists (alterative hypothesis). To construct a test statistics, we considered the cumulative sum (CUSUM), defined as $[\text{CUSUM}(t)] = \sum_{t'=1}^{t}(\theta_{t'} - \bar{\theta})$ with $t = 1, \cdots, n$ for the segment. It is expected that the total fluctuation of the CUSUM, $D = \max[\text{CUSUM}(t)] - \min[\text{CUSUM}(t)] \geq 0$, has a larger value if a CP is more likely to exist and D was therefore chosen as the test statistics in the CP detection. Next, the null distribution of D was constructed by randomly permuting the time order in the segment. In terms of the null distribution, we declared the existence of at least one CP if the null hypothesis can be rejected when a given confidence level, for example, 98%, was reached.

After declaring the existence of a CP, the most probable location of the CP in the segment was then identified as the time point whose left and right segments fitted by the corresponding mean values have the smallest total squared errors. Finally, the above procedures were repeated with binary segmentation to detect multiple CPs in the rotary trace as follows: For a long rotary trace, the most prominent CP with the largest D was located. The trace was then divided into two disjoint segments separated by the CP just found. The permutation test was then applied again to each of the disjoint segments to detect additional CPs. Such binary segmentation was repeated until no new CP can be found. Fig. S4*A* shows an example of the detected CPs (solid and dash vertical lines) for a rotary trace from the bMF$_1$(WT) with [ATPγS] = 1 mM. The angular histograms constructed from the raw rotary trace (blue line in inset of Fig. S4*B*) and the median trace from the CP intervals (red line in inset of Fig. S4*B*) are shown in Fig. S4*B*. One can see that the CP analyses denoise the rotary trace resulting in sharper peaks in the histogram.

Identification of *short pauses* using histogram of CP intervals. Some *short pauses* (~1 ms) detectable from CP analysis were observed (arrows in Fig. S4*A*) in the rotary traces. However, they were too short to be visible in both angular histograms of the raw rotary trace and the denoised trace (see Fig. S4*B*). In order to identify them, we constructed the histogram by counting

each CP interval's median angular value only once, regardless of its duration. Fig. S4*C* shows such histogram of CP intervals and 6 peaks can be clearly spotted.

Cleaning up procedure to remove undesired CPs hierarchically. CP detection finds not only the true CPs associated with state transitions, but also some extra CPs due to undesired fluctuations in the measurement, e.g., the dash vertical line in Fig. S4*A*. These extra CPs can affect the dwell-time statistics of the pauses since long pauses are broken into shorter segments. By assuming that the step-sizes of true state transitions should be larger than those from undesired fluctuations, we performed a systematic cleanup of the detected CPs as follows. Suppose a list of CP intervals with medians, $\tilde{\theta}_1, \tilde{\theta}_2, \tilde{\theta}_3, \cdots$, and median absolute deviation (MAD), $M_1, M_2, M_3, \cdots$ are obtained from the CP detection. The MAD, defined as $M_a = \text{Median}\big(\big|\theta_1 - \tilde{\theta}_a\big|, \big|\theta_2 - \tilde{\theta}_a\big|, \cdots, \big|\theta_n - \tilde{\theta}_a\big|\big)$ for the *a*-th CP interval with *n* data points and median $\tilde{\theta}_a$, quantifies the variation of angular fluctuation of a CP interval. The median and MAD were considered here instead of the mean and standard deviation since they do not assume the noise to be Gaussian and are insensitive to outliers. With this setting, two consecutive (e.g., the *a*-th and (*a*+1)-th) CP intervals were combined (or the CP between them is removed) if the difference of their median angles are smaller than the sum of the MADs of the two CP intervals times a constant *A*, i.e., $\big|\tilde{\theta}_a - \tilde{\theta}_{a+1}\big| < A \cdot (M_a + M_{a+1})$. Here $A \geq 0$ is a control parameter to adjust how many consecutive CP intervals are combined (or how many CPs are removed). A larger (smaller) *A* results in removing more (less) CPs.

In the cleanup procedure, we started from a small *A* to remove only a few CPs. The remaining CPs then give us a revised denoised trace, and the squared error between the original rotary trace and the revised denoised trace was evaluated. The evaluation of squared error as a function of *A* was then repeated by increasing *A*. When *A* is small, only CPs associated with the small undesired fluctuations were removed so that the squared error increases slowly as *A* increases (yellow region in Fig. S4*D*). On the other hand, when *A* increases to a certain value such that CPs associated with real state transitions were removed, the squared error begins to increase rapidly (gray region in Fig. S4*D*). The appropriate *A* therefore locates just before the rapid increasing of the squared error.

After removing the undesired CPs, the histogram of CP intervals can be constructed again. Fig. S4*E* shows that the histogram of CP intervals after the cleanup procedure is further sharpened compared with Fig. S4*C* and 6 peaks can be separated easily, e.g., by the dash vertical lines in Fig. S4*E*.

Determining the stepsize from *longer pause* to *shorter pause*. After the extra CPs were removed and the 6 peaks in the histogram of CP intervals corresponding to the 6 pauses (3 *longer* and 3 *shorter pauses*) in the rotary trace were identified, each CP interval in the rotary trace was then assigned to the corresponding catalytic pauses. As a result, the angular differences between the current and next *longer pause* (denoted by $\theta_{long-long}$ in Fig. S4*F*), and those between the current hydrolysis pause and the next *shorter pause* (denoted by $\theta_{short-long}$ in Fig. S4*F*) were evaluated by the difference of the median angle of the corresponding CP intervals along the rotary trace. Since the measured angular difference $\theta_{long-long}$ may be different from 120° for each of the 3 *longer pauses* due to the tilting of the imaging plane, the stepsize between the current *longer* and the next *shorter pauses* were estimated by the set of ratios $\theta_{short-long}/\theta_{long-long}$ from the rotary traces. Finally, the distribution of $\theta_{short-long}/\theta_{long-long}$ was constructed from which the median value of $\theta_{short-long}/\theta_{long-long}$ and its error (represented by the bootstrap 68% bootstrap confidence interval) can be evaluated.
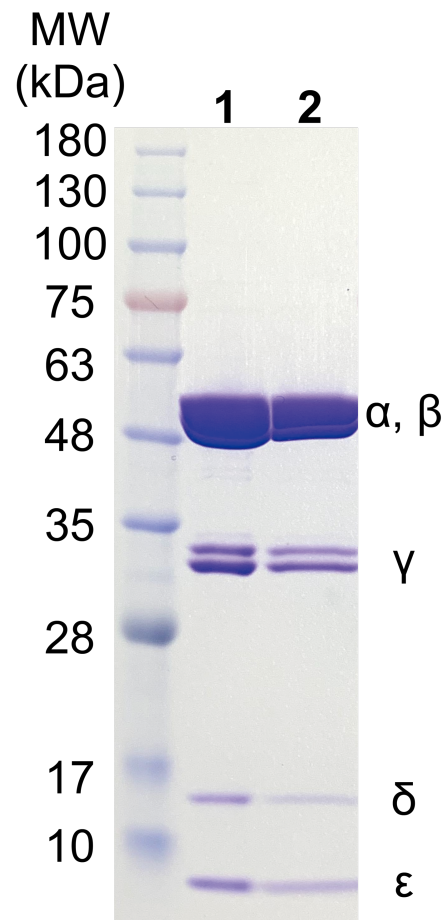
Fig. S1. SDS-PAGE analysis of *b*MF₁.

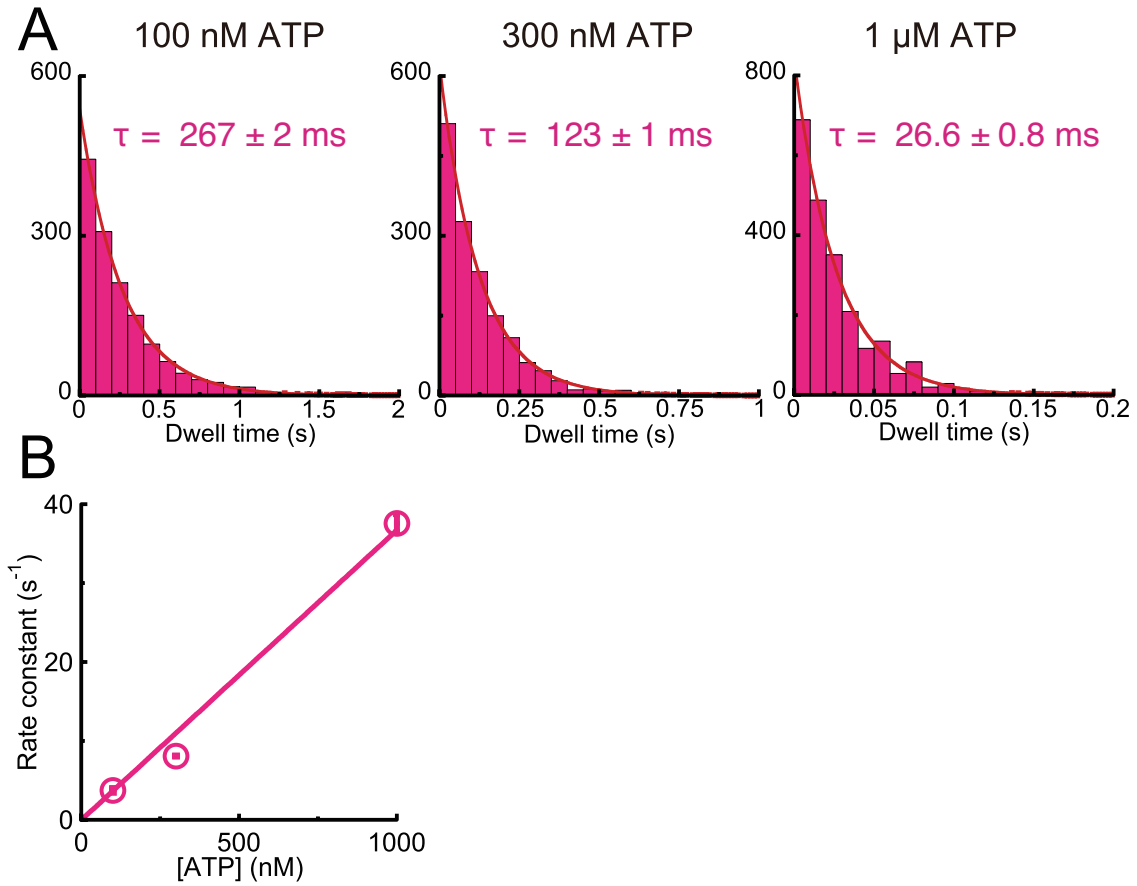(Lane 1) The reference sample without dilution. (Lane 2) The sample after 1000-times dilution and re-concentration.

Fig. S2. Dwell time analysis at low [ATP]s (recording rate: 125-500 fps).

(*A*) Histograms of dwell time at various [ATP]s (N = 3-5). Values are fitted parameter ± fitting error. (*B*) [ATP] versus rate constants of ATP binding.
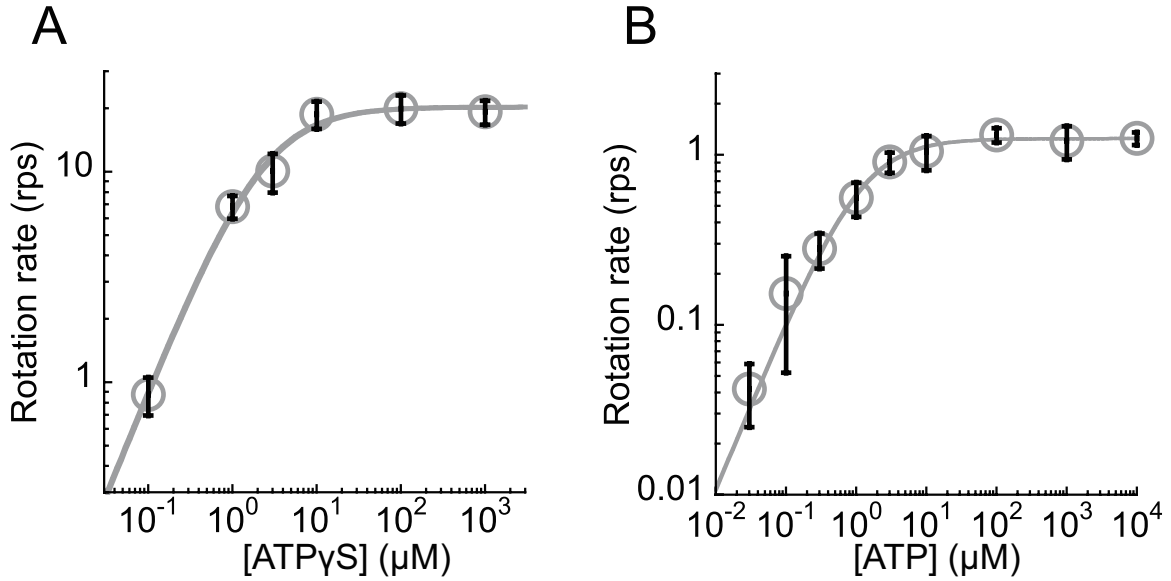
Fig. S3. [ATP or ATPγS] versus rotation rate

(*A*) ATPγS-driven rotation of bMF$_1$(WT) with V_{max} and K_m of 20.3 ± 1.0 rps, and 2.2 ± 0.5 μM (N = 21-27). (*B*) ATP-driven rotation of bMF$_1$(βE188D) with V_{max} and K_m of 1.24 ± 0.03 rps, and 1.15 ± 0.13 μM (N = 19-34). The mean value and the SD for each data point are shown as gray circles and black error bars. The gray line represents the Michaelis-Menten fitting. Values are fitted parameter ± fitting error.
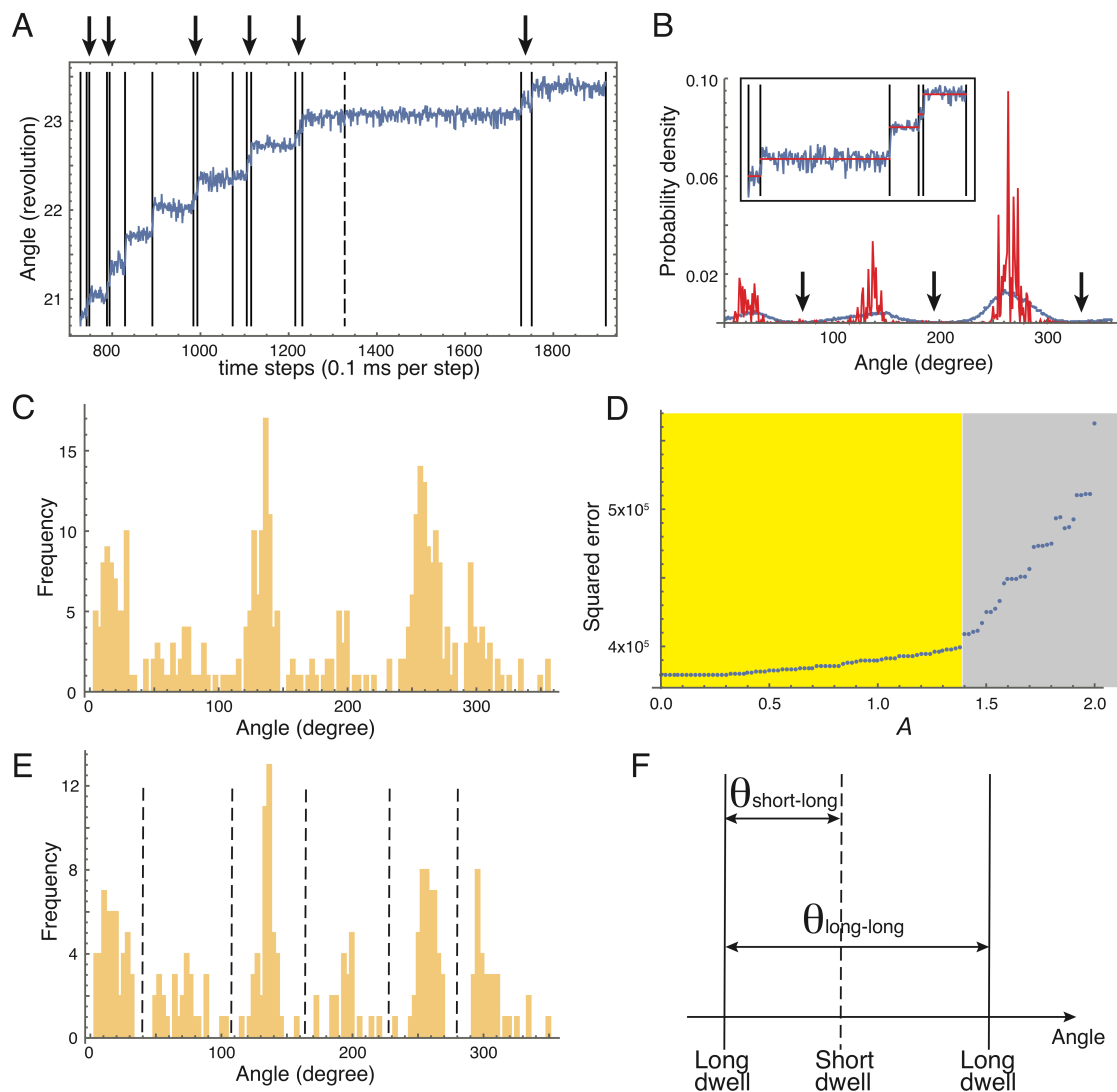
Fig. S4. Statistical analysis of rotary trace to determine the number of pauses and stepsizes.

(*A*) Example of rotary trace and results of CP detection. Solid and dashed vertical lines are CPs due to state transitions and undesired fluctuations, respectively. Arrows indicate *short pauses* (~ 1 ms) that can be detected by CP analysis. (*B*) Angular histogram constructed from the raw trace (blue) and the denoised trace (red) from the CP detection. Arrows show the angular regions where the short pauses in (*A*) locates but they are too short to be visible in the histogram. An example of raw and denoised traces is shown in the inset. (*C*) Histogram of CP intervals where each CP interval was only counted once regardless of its duration. 6 peaks are now clearly visible. (*D*) Squared error plotted as a function of *A* to determine how many CPs to be removed in the cleanup procedure. The yellow region corresponds to the range of *A* where only CPs due to undesired fluctuation were removed, whereas the gray region corresponds to the range of *A* where CPs associated with true state transitions were also removed. (*E*) The histogram of CP intervals after

the cleanup procedure shows sharper peaks and the 6 pauses can be easily separated as indicated by the dashed lines. (*F*) The determination of the stepsize between the current *long pause* and the next *short pause*. Since the observed angular difference from the current to the next *long pauses* may not be 120° due to possible tilting of the imaging plane, the ratio $\theta_{short-long}/\theta_{long-long}$ is considered in this study.
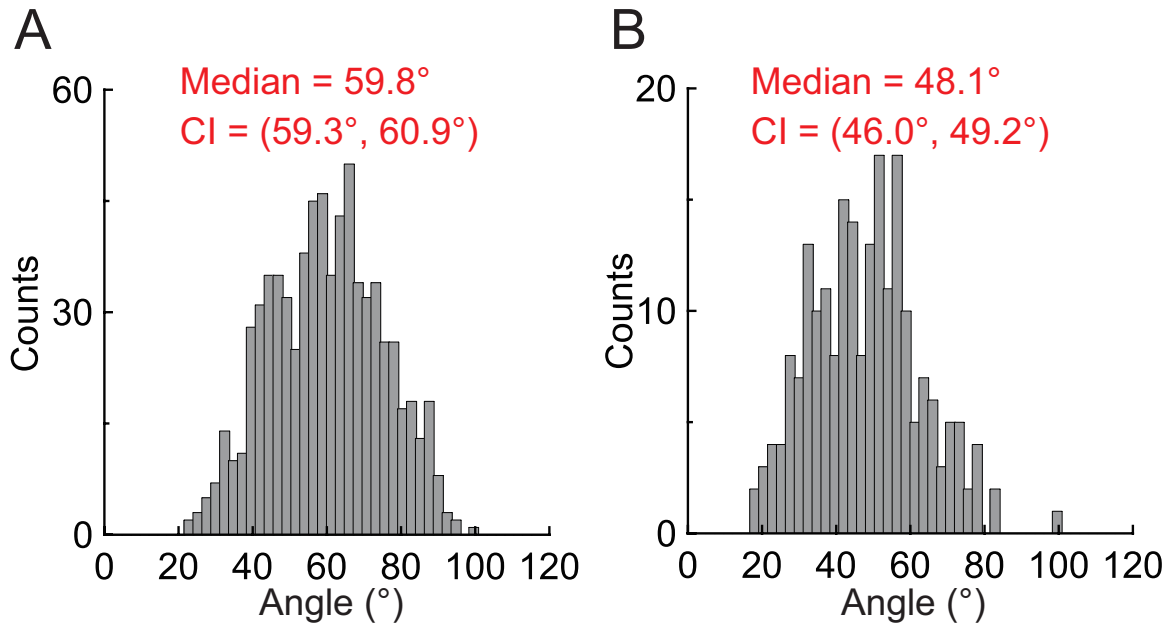
Fig. S5. Histograms of the angle position of *short dwell* from *long dwell*.
(*A*) 1 mM ATPγS in *b*MF$_1$(WT) (727 steps, 15 molecules). (*B*) 1 mM ATP in *b*MF$_1$(βE188D) (215 steps, 10 molecules). Values are the median angle and the 68% bootstrap confidence intervals (CI), respectively.
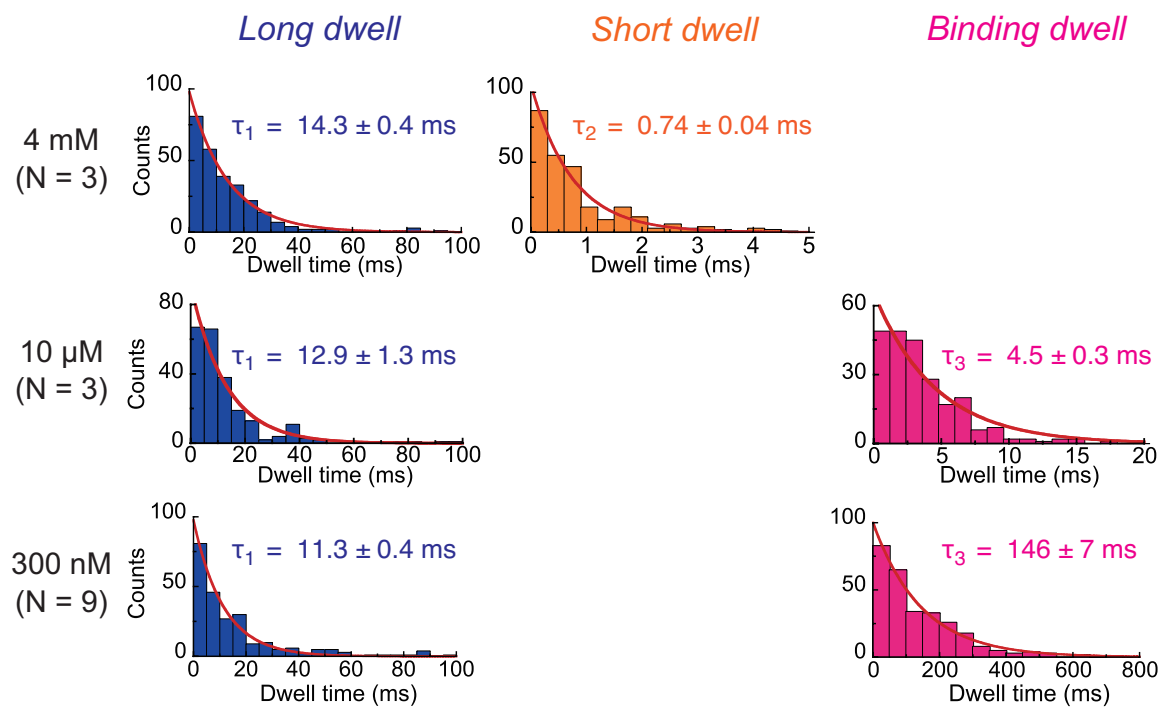
Fig. S6. Dwell time analysis of *long, short,* **and** *binding dwell* **at indicated [ATPγS]s in** *b***MF₁(WT) (values are fitted parameter ± fitting error).**
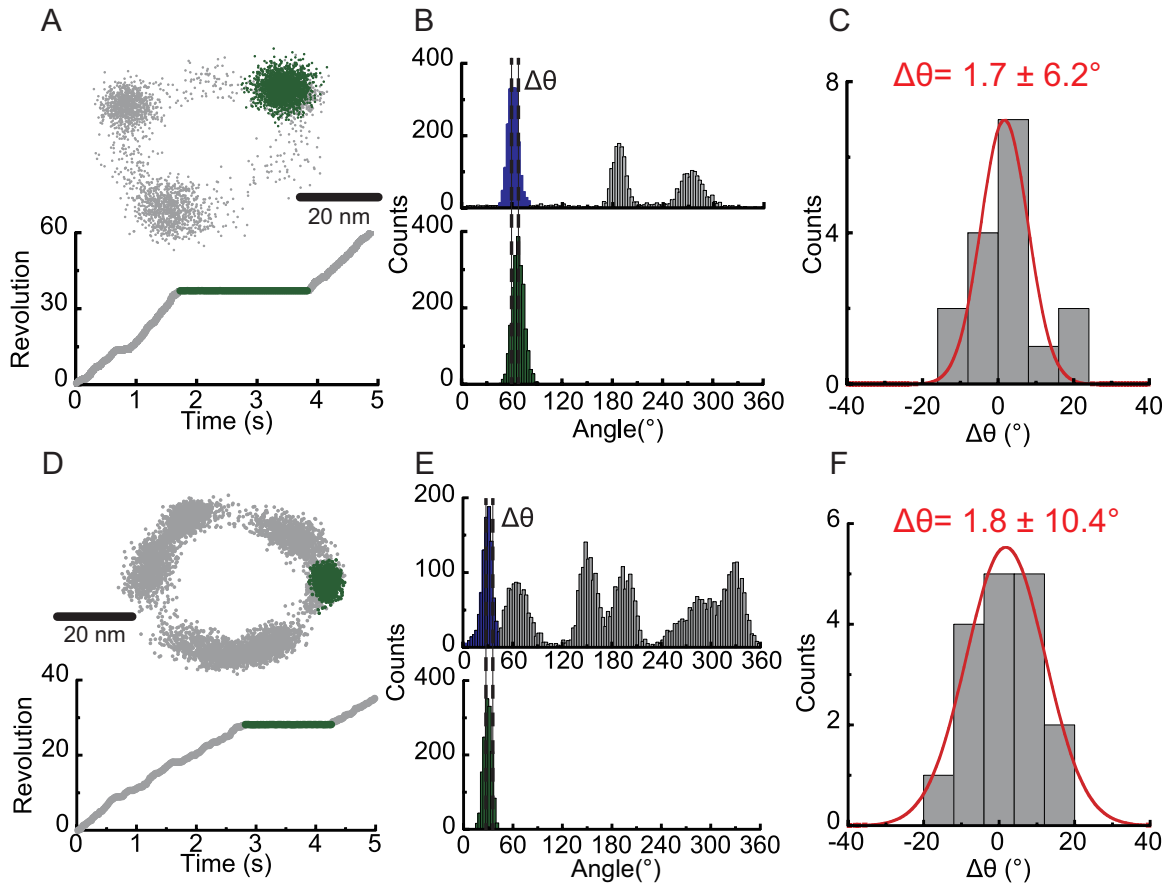
Fig. S7. Analysis of ADP-inhibited pauses (green) observed in 1 mM (*A*)-(*C*) and 1 μM ATPγS (*D*)-(*F*) (recording rate: 1k fps).

(*A*), (*D*) x-y plot and time course of a representative molecule. (*B*), (*E*) Angle histograms of rotation (upper) and inhibited state (lower). Δθ is defined as the distance between ADP-inhibited pause (green) and *long dwell* (blue). (*C*), (*F*) The angular histogram of Δθ (N = 16 in (*C*) and N = 17 in (*F*)). Values are mean ± SD.
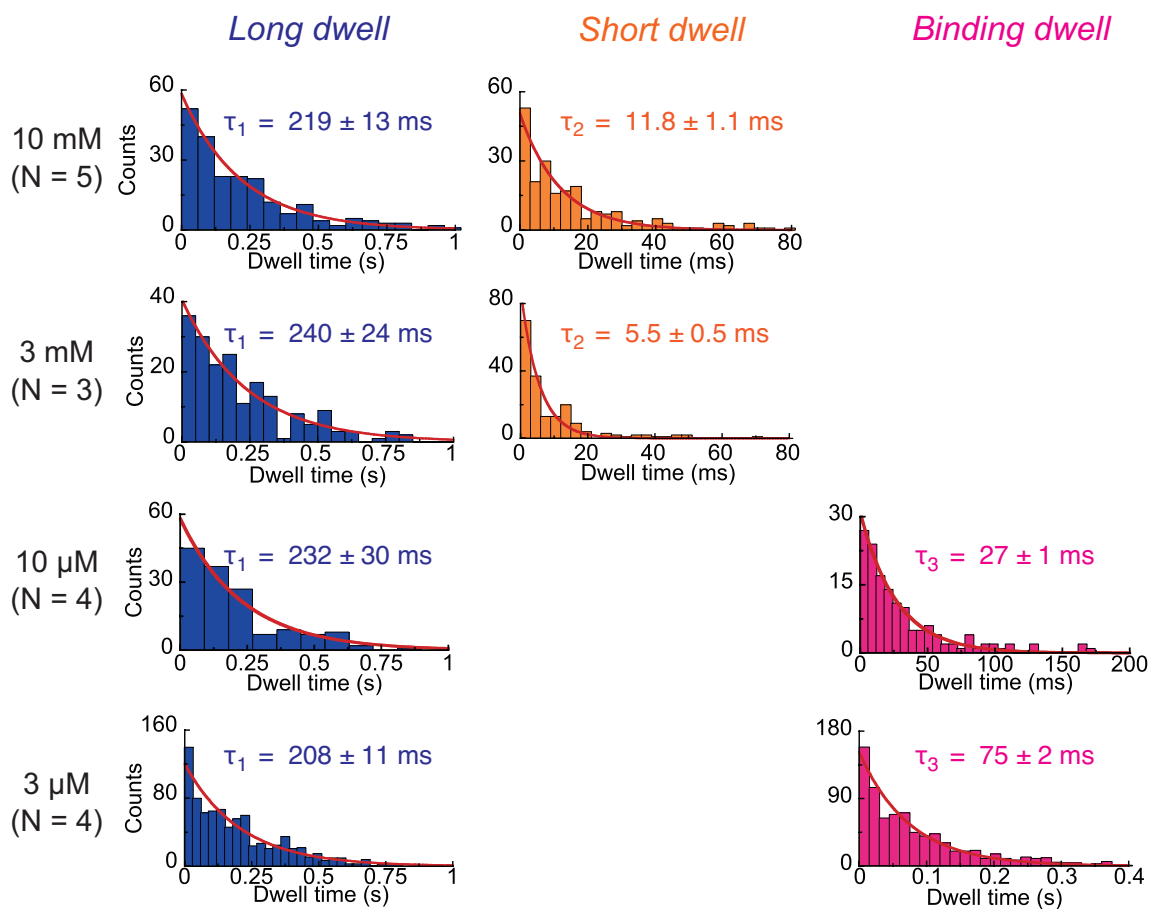
Fig. S8. Dwell time analysis of *long, short,* and *binding dwell* at indicated [ATP]s in *b*MF₁(βE188D) (values are fitted parameter ± fitting error).
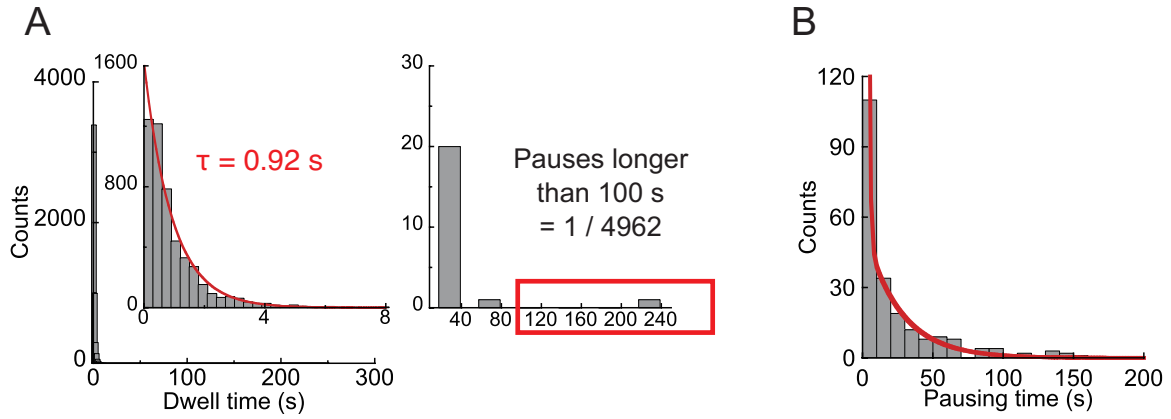
Fig. S9. Kinetic analysis in the absence of AMP-PNP.

(*A*) Dwell time analysis at 100 nM ATP (4962 dwells, 3 molecules). (Left) Dwells shorter than 8 s. The time constant was estimated to be 0.92 s. (Right) Dwells longer than 8 s. ADP inhibition rarely occurred in this condition. (*B*) Distribution of pausing times before resuming the rotations at 2 mM ATP. The histogram was fitted with a double exponential decay function; $y = N_{sp} \exp(-t/\tau_{sp}) + N_{lp} \exp(-t/\tau_{lp})$, as previously described (2). τ_{sp} and τ_{lp} were estimated to be 1 s and 25 s, respectively.
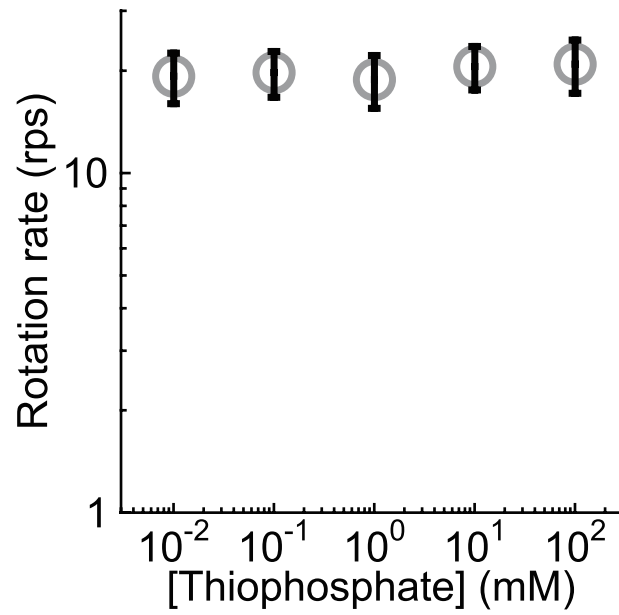
Fig. S10. Rotation rate at 1 mM ATPγS with various [thiophosphate]s.

The mean value and the SD for each data point are shown as gray circles and black error bars, respectively (N = 22-27).

Table S1. Angle dependence of kinetic parameters determined in Fig. 6 (values are fitted parameter ± fitting error).

	Angle dependence
$k_{on}^{ATP}(M^{-1}s^{-1})$	$(9.4 \pm 0.4) \times 10^6 \times \exp[(0.049 \pm 0.002) \times \theta]$
$k_{off}^{ATP}(s^{-1})$	$(0.12 \pm 0.01) \times \exp[-(0.012 \pm 0.002) \times \theta]$
$K_a^{ATP}(M^{-1})$	$(6.6 \pm 0.6) \times 10^7 \times \exp[(0.072 \pm 0.003) \times \theta]$
$K_d^{ATP}(M)$	$(1.0 \pm 0.2) \times 10^{-8} \times \exp[-(0.070 \pm 0.007) \times \theta]$
$k_{hyd}^{ATP\gamma S}(s^{-1})*$	$(0.12 \pm 0.01) \times \exp[(0.015 \pm 0.002) \times \theta]$
$k_{syn}^{ATP\gamma S}(s^{-1})*$	$(0.19 \pm 0.01) \times \exp[-(0.008 \pm 0.001) \times \theta]$
$K_E^{Hyd-ATP\gamma S}*$	$(0.59 \pm 0.03) \times \exp[(0.028 \pm 0.001) \times \theta]$

*Determined using a mutant, bMF₁(βE188D)

References

1. Li CB, Ueno H, Watanabe R, Noji H, Komatsuzaki T (2015) ATP hydrolysis assists phosphate release and promotes reaction ordering in F_1-ATPase. *Nat Commun* 6:1–9.
2. Hirono-Hara Y, et al. (2001) Pause and rotation of F_1-ATPase during catalysis. *Proc Natl Acad Sci* 98(24):13649–13654.